Appl. Phys. B 57, 65–82 (1993)

Applied Physics B Photophysics and Laser Chemistry

Monitoring Air Pollution Related Meteorology Using SODAR

State of the Art

S. P. Singal

National Physical Laboratory, New Delhi - 110 012, India

Received 4 January 1993/Accepted 9 April 1993

Abstract. Hazardous situations in air pollution can many a times be avoided in case short term local weather forecasting of the boundary layer meteorology becomes available. Amongst the various remote sensing techniques, it has been seen that acoustic remote sensing (SODAR) of the lower atmosphere can be employed to determine and predict the atmospheric boundary layer meteorological parameters. In specific, information can be obtained about thermal stratification, mixing height, low level disturbances, depth of the planetary boundary layer, stability classification, wind velocity, wind variances, turbulence parameters, and diffusion characteristics etc. when SODAR is used in conjunction with surface level measurements of the usual meteorological parameters.

In the paper a brief description of the acoustic remote sensing technique and a review of the work done during the last two decades to determine the various air quality related meteorological parameters has been given. The methodology to determine mixing height, stability classification and diffusion and dispersion characteristics using mostly the information from the SODAR echograms has also been described. The SODAR echograms obtained at Delhi for the period May 1977 to April 1982 have been processed and analyzed using pattern recognition to determine these parameters. Doppler SODAR information of wind speed and direction have not been treated for the above purpose. Using the Gaussian dispersion model, pollution concentration downwind of a emission source (in the present case it is a cement factory at Nimbahera, Chittorgarh, India) has also been computed with the help of SODAR determined data. It has been found that measured values with the help of high volume sampler conform to the estimated pollution concentration. A peak in the value of the estimated pollution concentration during the fumigation period has also been seen.

PACS: 92.60.Ek, 43.85.+f, 92.60.Sz

A_r	Area of the receiving antenna
D	Stack diameter [m]
F	Vertical flux of the buoyant plume
K	von Karman's constant equal to 1.4
L	Monin-Obukhov length [m]
L_a	Acoustic attenuation along the path inclusive of the transducer efficiencies
P	Ambient air pressure [hPa]
P_0	Total pressure [hPa]
P_r	Received acoustic power
P_t	Transmitted acoustic power
Q	Quantity of stack emission per unit time [g s^{-1}]
Q_0	Surface heat flux
R	Range to the scattering volume [m]
R_i	Richardson number
R_s	Inner stack radius at the top [m]
R_{if}	Flux Richardson number
T	Ambient air temperature [K]
T_s	Average temperature inside the stack [K]
U	Horizontal wind speed [m s^{-1}]
U_z	Horizontal wind speed at the stack height [m s^{-1}]
V_s	Average exit velocity at the stack top [m s^{-1}]
Z	Depth of the mixed boundary layer, i.e. the height of the atmospheric boundary layer [m]
Z_i	Inversion height, i.e. the distance between the ground and the base of the elevated inversion [m]
Z_0	Length parameter of roughness [m]
a	Empirical constant equal to 1.5 in stable conditions and 10 in unstable conditions
b	Empirical constant equal to 1 in stable conditions and 10 in unstable conditions
c	Velocity of acoustic waves in air [m s^{-1}]
d	Distance from source to receptor [m]
h	Mixing depth as per Holzworth model [m]
h_e	Effective stack height [m]
Δh	Plume rise height [m]
g	Acceleration due to gravity

k Wave number
m A constant equal to 0.45
p A variable number for the various stabilities
w Vertical wind velocity [m s^{-1}]
w' Fluctuations in vertical wind velocity [m s^{-1}]
w_* Mixed layer velocity scale
x, y, z The three coordinates [m]
$3.5x^*$ Distance to the point downwind of the stack where the plume is no longer rising
z_0 Measure at the surface level [m]
z_s Depth of the thermal plumes on the sodar echograms [m]
C_e^2 Humidity structure parameter
C_m^2 Concentration structure parameter
C_n^2 Refractive index structure parameter
C_T^2 Temperature structure parameter
C_v^2 Velocity structure parameter
C_p Specific heat at constant pressure
C_{eT} Cross correlation structure coefficient of temperature and humidity
α Constant approximately equal to 1.4
β Constant equal to 6
ϱ Density of air
ψ Pollution concentration [g m^{-3}]
τ Transmitted pulse length
$\odot$ Potential temperature
$\odot'$ Fluctuations in potential temperature
θ Scattering angle
ϕ_{max} Martin's function
σ_R Ratio of backscatter to forward scatter intensities from the same volume
σ_W Standard deviation of the vertical wind velocity [m s^{-1}]
σ_y Cross wind dispersion coefficient
σ_z Vertical dispersion coefficient
σ_ϕ Standard deviation of the vertical wind direction [deg]
σ_θ Standard deviation of the horizontal wind direction [deg]
$\sigma(\theta)$ Scattering cross section at angle

The rapid growth of industries and urban centres, coupled with the extraordinary accomplishments of modern technology during the last few decades, though responsible for a higher standard of living, has also become a cause of strong public concern because of the discharge of various types of hazardous and toxic gaseous and particulate matter in the atmosphere, which are altering the environmental quality of life at micro, macro and global levels. The air quality parameters of our environments are thus required to be monitored for necessary prediction and control.

Monitoring of ambient air quality can be carried out by the measurement of various air pollutants present in the atmosphere as also through monitoring of the atmospheric boundary layer meteorology assuming that the number and distribution of the sources of air pollution remain the same. In the latter case, low level stability, inversion topography, buoyancy, turbulence strength, mixing height, wind velocity, and meso-scale flow patterns are some of the meteorological parameters that need to be monitored.

Often conventional in situ techniques such as radio sonde, instrumented tower, tethered balloon, and instrumented aircraft etc. are used to monitor the essential atmospheric parameters. Out of these radiosonde is the most common in situ technique. Typical data consist of twice daily profiles of temperature, pressure, humidity, and wind at a place mostly in the vicinity of the airport. These data supported by hourly observations of surface parameters of pressure, wind, temperature, humidity, visibility, and cloud cover help to interpolate and extrapolate stability, mixing depth and wind profiles in the lower atmosphere. However, available information is generally limited at the lower levels and is not adequate for air quality monitoring and forecasts since aviation requirements have often dictated the location of the sensors at sites which are not necessarily in the best interests of the air quality meteorologists. Slow ascent radiosonde or tethered balloon systems, instrumented towers and instrumented aircrafts can help to collect low level data to some extent but it may be difficult to afford the increase in the density of observations using these instruments, as the cost will increase enormously.

Remote sensors, in comparison to the in situ sensors, can provide data for the atmospheric parameters at lower heights continuously in both space and time and with higher resolution. They depend on the propagation characteristics of acoustical, optical and electromagnetic waves in the medium. Many of the remote sensing devices have the ability to scan rapidly large regions in three dimensions. Others can give line integrals of certain parameters giving spatially averaged values that may be nearer to the desired measurement.

Considering the overall cost of the system, availability of tracers, large scattering cross-section, stage of development, and reliability of measurements during the last two decades, it is felt that the measurement system can be made up entirely of an acoustic device [1–5]. The interaction of sound waves with the inhomogeneities of the lower atmosphere is very much stronger [1] than that of the electromagnetic spectrum as shown in Table 1. It is seen that 1 K fluctuation in temperature is equivalent to about 1700 N units change in sonic refractive index (1 N unit equals 1 part in 10^6) compared to only 1 N unit change in optical and radio refractive index. Similarly 1 m s^{-1} variation in wind speed is equivalent to 3000 N units change in acoustic refractive

Table 1. Refractive index variations per unit change in the characteristic parameters of the atmosphere (Data from [1])

Magnitude of parameter change	Change in refractive index N Unit ($N = 10^{-6}$)		
	Acoustical	Radio	Optical
1 K fluctuation in temperature	1700	1	1
1 m s^{-1} variation in wind speed	3000	2×10^{-6}	2×10^{-6}
1 hPa change in water vapour pressure	140	4	0.04

index compared to practically no change in the refractive index of electromagnetic waves. Further 1 hPa change in water vapour corresponds to about 140 N units change in acoustic refractive index compared to only 4 N units change in radio refractive index and 0.04 N unit change in optical refractive index. These changes in the refractive index for acoustic waves compared to that for electromagnetic waves, make the scattering efficiency of turbulence one million times greater for acoustic waves than for electromagnetic waves.

1 Acoustic Sounding

Gilman et al. [6] were the first to report successful experiments in atmospheric acoustic sounding. McAllister [7] was the first to display real time backscatter echoes on the facsimile machines. Little [1] was the first to perform comprehensive system analysis on the functioning of acoustic sounding system. This was followed by a major research and development effort in acoustic sounding systems by NOAA Wave Propagation Laboratory, Boulder, Colorado, USA, and at a number of other places in the world.

Acoustic sounder (SODAR) popularly called 'Acoustic Radar' functions like an active sonar or a pulsed radar system. Highly directional short bursts of sound energy in the audio frequency range 1500 Hz to 10000 Hz are radiated into the atmosphere. These waves get scattered during their propagation in the atmospheric air from fluctuations in temperature, wind speed and humidity of eddy sizes within the inertial subrange and are received (Fig. 1) either by the same antenna (monostatic or backscattering mode) or by another antenna (bistatic or forward scattering mode). The information contained therein is processed and stored and also displayed on the facsimile chart. Useful qualitative and semi-quantitative information about the ground based thermal activity, nocturnal inversions and symmetric and asymmetric waves can be seen on the facsimile chart while quantitative information about velocity and temperature structure parameters, turbulence intensity and wind field in the scattering volume at various heights in the atmospheric boundary layer can be computed by measuring the amplitude and frequency of the received scattered signal.

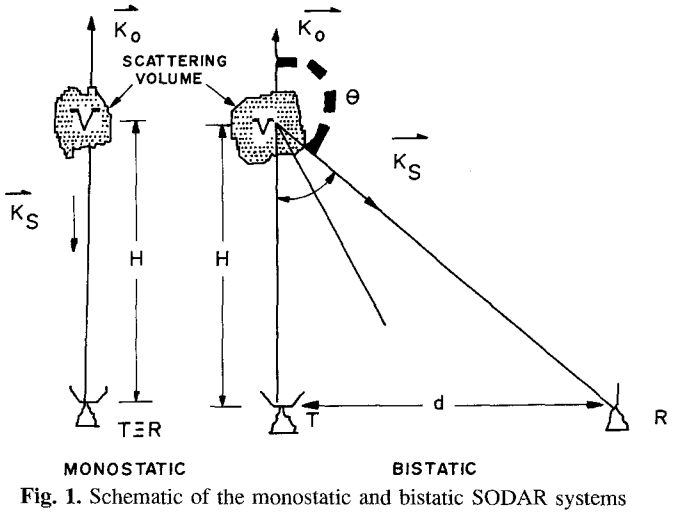

Fig. 1. Schematic of the monostatic and bistatic SODAR systems

The scattering cross-section at an angle θ from the original direction of the sound waves in the inertial subrange can be expressed as:

$$\sigma(\theta) = 1.52k^{1/3}\cos^2\theta\left[0.13C_n^2 + \frac{C_v^2}{4c^2}\cos^2(\theta/2)\right] \times \left[2\sin(\theta/2)\right]^{-11/3},$$

where k is the wave number of the transmitted sound waves, c is the sound velocity ($\mathrm{m\,s^{-1}}$), C_v^2 is the wind velocity structure parameter and C_n^2 is the structure parameter of refractivity which depends on temperature and water vapour fluctuations and according to Wesely [8] can be expressed as:

$$C_n^2 = \frac{C_\mathrm{T}^2}{4T^2} + 2(0.307)\frac{C_\mathrm{eT}}{4PT} + (0.307)^2\frac{C_\mathrm{e}^2}{4P^2}.$$

Here T and P are the mean temperature (K) and pressure (hPa) of the air respectively, C_T^2 and C_e^2 are the temperature and humidity structure parameters respectively and C_eT is the cross correlation structure coefficient of temperature and humidity. For backscattering, the scattering angle becomes 180° which reduces the scattering cross section to:

$$\sigma(\Pi) = 0.016k^{1/3} \times \left[\frac{C_\mathrm{T}^2}{4T^2} + 2(0.307)\frac{C_\mathrm{eT}}{4PT} + (0.307)^2\frac{C_\mathrm{e}^2}{4P^2}\right].$$

From the above equations, it can be thus seen that backscattering is due to temperature and humidity inhomogeneities, it is sensitive to eddies of sizes equal to and above half the transmitted wavelength, there is no scattering at 90° and forward scatter is stronger than that of backscatter. Thus SODAR has the capability to give information about thermal structure, turbulence parameters and wind vector profile in the lower atmosphere as a function of time and height. Since these parameters are of importance in air pollution dispersion, in this paper the acoustic remote sensing technique (SODAR) is described to monitor the air quality related meteorological parameters at a place. SODAR echograms have been used for the present studies, and horizontal wind speed and direction have not been treated.

2 Studies of Thermal Structure

SODAR echograms depicted on the facsimile records are broadly classified as shear echoes and thermal echoes (Fig. 2). Shear echoes tend to be horizontal and are caused by turbulence in regions of static stability (potential temperature increasing with height). They may be surface based, aloft and stratified. Thermal echoes appear in the form of stalagmites like structures rising from the ground and are caused by turbulence in the unstable, super adiabatic layer of the atmosphere (potential temperature decreasing with height). They occur when the surface is appreciably warmer than the air aloft. The intermittent groups of thermal echoes mark individually rising convective cells called thermals and the echo free regions between thermals represent neutral or adiabatically descending air.

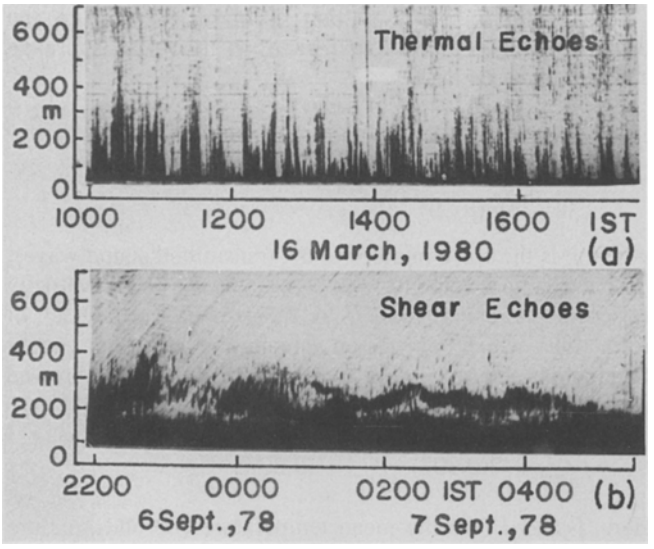

Fig. 2. The two types of characteristic SODAR structures – thermal echoes and shear echoes. Data from SODAR installed at the National Physical Laboratoy (NPL), New Delhi (India)

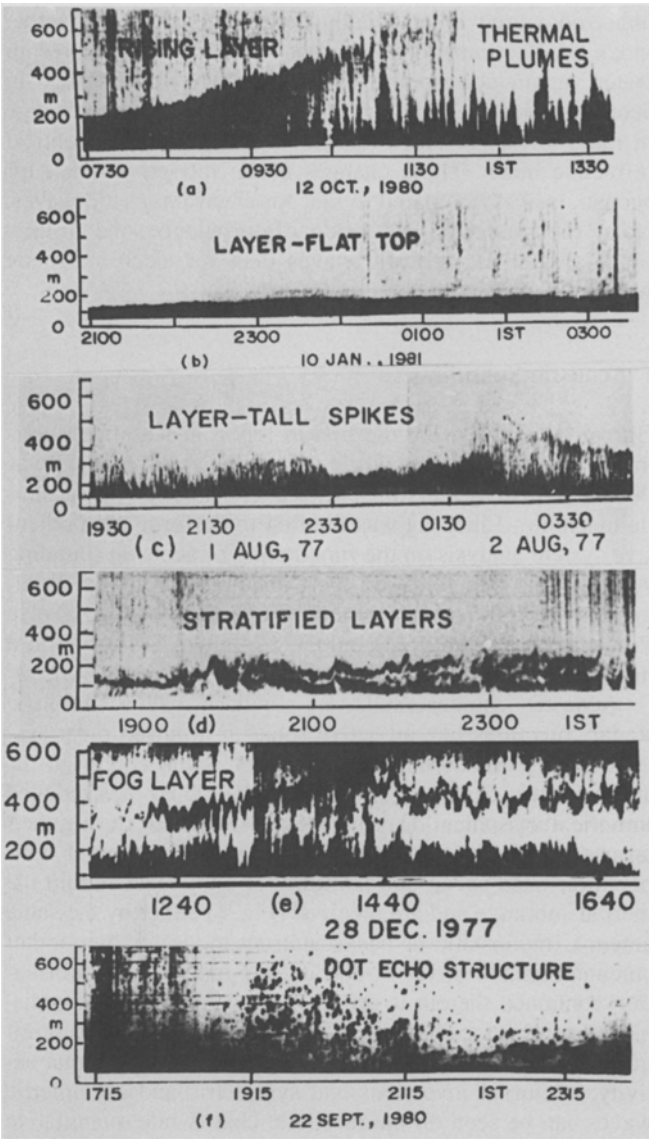

Fig. 3. Typical thermal structures observed in the NPL monostatic SODAR system

The day-to-day structures observed on sodar echograms (Fig. 3) are, however, not always as simple as seen in Fig. 2, but they can always be linked with these broad categories. The variations or the complexity of these structures represent the prevailing changed meteorological conditions of the atmosphere. In the morning, solar heating erodes the nocturnal surface based stable layer forming ground based thermal plumes capped by the rising stable layer (Fig. 3a). With continuous solar heating, the stable layer rises sufficiently high so that either it goes beyond the detection range of the sounder or it loses sufficient turbulence to become insensitive to SODAR detection and thus thermal plumes prevade on the SODAR echograms. Height and rate of occurrence of thermal plumes become maximum by the afternoon after which they start decreasing in accordance with the fall in solar heat flux.

During night time, under slight or no wind conditions, strong short range echoes having an abrupt but almost uniform upper limit exhibiting a nearly flat top layer (Fig. 3b) are formed. Thickness of these layers may slightly increase with time. Medium to strong surface winds bring in mixing within the stable layer resulting in random spiky structures at the top (Fig. 3c). Turbulent weather conditions and even clear sky conditions have been seen to develop, sometimes, a stratified/multilayer or elevated layer structure (Figs. 3d–f) with or without undulations superposed over them. Multiple layers represent stable shear structure under light wind conditions or advection of superimposed flow due to some meso-scale weather phenomena. Elevated layer represents the presence of fog layer, subsidence inversion, marine boundary layer or some other approaching/persisting turbulent weather condition.

Undulations have been seen under calm to medium wind conditions as also before and after the occurrence of thunder storms under medium to strong wind conditions. The undulating structures may either exhibit features of symmetric sinusoidal wave motion under clear weather conditions or they may show slightly unsymmetric rounded saw-tooth type wave motion under turbulent weather conditions. These waves have periods of the order of a few minutes and amplitude in the range of 100 m peak to peak [9]. It seems that these undulations represent gravity waves developed in regions separating two air masses of different density and wind vector and are associated either with convective stability during the fumigation period or with wind shear variations under stable layers conditions. Enhanced wind shear, a characteristic of stable layers, maintains turbulence through all or part of its depth against vertical stability and is observed through interrogating sound waves by reflection at selected scale lengths of turbulence of half the acoustic wavelength.

3 SODAR Studies of Atmospheric Stability

Amongst the early workers, Beran et al. [10] were the first to demonstrate the potential of the acoustic sounding device for making continuous meso-scale measurements in

critical air pollution situations. Subsequently, Tombach et al. [11] showed relevance of the acoustic sounding technique to obtain information on atmospheric stability, height of elevated inversion, depth of mixed layer, and turbulent eddy scale size in thermal plumes, data useful for dispersion and diffusion modeling of atmospheric pollutants. Various approaches of this nature have also been made by other investigators from time to time to draw information about air pollution related meteorological parameters from SODAR data. The following, in brief, are some of the methodologies used to draw air pollution related meteorological information from SODAR data.

3.1 Pattern Recognition Technique

The repeatable patterns on the SODAR echograms have been studied by many workers in the field from time to time, to determine from their characteristic behaviour and nature, the stability of the atmosphere. Shaw [12] was the first who identified the repeatable patterns and was followed by Fukushima [13, 14], who gave summary charts of the observed facsimile patterns and distinguished three general characteristic echo patterns apart from regions of no echo, wind, rain, and ambient noise. Schubert [15] proposed a system of 15 categories to identify the various phenomena of climatological interest. Clark et al. [16] proposed a numerical classification scheme of 14 different types and separated cases of surface based echoes from elevated echo layers and related them to the boundary layer meteorological conditions.

Hall [17] introduced computer compatible coding to the various SODAR structures together with numerical notation of the height of the structure. This made it possible to collect numerical information about the climatology of the planetary boundary layer at a site under investigation, than was possible by other classification schemes.

Prater and Colls [18] developed a categorization scheme similar to Clark et al. [16], but they identified only five major categories of sounder structures. In their scheme of categorization, they did not include any identification for zones of no echoes and non-recognizable noisy echoes. Their scheme did not even recognize a discrete category for each of the multiplicity of the atmospheric structures normally observed on the acoustic sounder echograms. The diurnal variations of the probability of occurrence of any one stability class were studied and relationships were shown to exist between acoustic sounder stability category and pollution related meteorological parameters.

Maughan [19] and Maughan et al. [20] developed a numerical code to classify the various types of SODAR echoes. The successive digits in the scheme gave information about the height of the structure with the scheme identifying the type and height of the inversion layering and also their complexity. This classification scheme was also adopted by Asimakopoulos et al. [21] to study stability frequencies in different cities in Greece. A code of eight numbers including no-echo and no-reliable-echo conditions was introduced.

Walczewski [22–24] and Walczewski and Felesky-Bielak [25] considered four basic characteristic forms of SODAR echoes, vertical (type 1), ground-based horizontal layer (type 2), elevated horizontal layer in the absence of ground-based layer (type 3), and no-echo structure (type 4). Type 1 culminated at noon, type 2 at midnight, type 3 in the morning, and type 4 in the evening around sunset time. Digital representation or coding was introduced and the SODAR echogram were interpreted in terms of atmospheric stability categories following the variations in the vertical temperature gradient as criteria to define the stability classification.

Singal et al. [26–29] developed an approach based on SODAR echo patterns to classify Pasquill stability categories. Simultaneously measured datas of standard deviations of the horizontal wind direction were used to determine Pasquill stability classification to correlate with SODAR deduced

Table 2. Classification of SODAR echograms in terms of stability categories

S.N.	Stability class (Pasquill)	Wind direction fluctuation criteria (degrees)	Nature of SODAR echograms	Outlook
1.	Strongly unstable (A)	$\sigma_\theta \geq 23$	i) Well defined thermal plumes up to heights more than or equal to 275 m	Clear sunny day with strong solar heating and light/calm winds
2.	Moderately unstable (B)	$18 \leq \sigma_\theta < 23$	i) Well defined thermal plumes up to shallow heights (less than 275 m) ii) Rising layer with thermal plumes below	Moderate solar heating and moderate winds Bright sunny morning
3.	Slightly unstable (C)	$13 \leq \sigma_\theta < 18$	i) Thermal plumes up to very shallow heights	Weak solar heating, cloudy day, moderate to strong winds, and late afternoon
4.	Neutral	$8 \leq \sigma_\theta < 13$	i) Spiky top layer of height above 150 m ii) No structure iii) Darkness due to rain or wind-induced noise	Early evening hours on clear days. After rain or storm, cloudy/windy conditions. During rain or heavy winds (storm)
5.	Slightly stable (E)	$4 \leq \sigma_\theta < 8$	i) Flat top layer of depth more than 100 m ii) Surface-based layer with spiky, top of depth generally within 150 m iii) Stratified layers of depth more than 200 m	Clear night with moderate winds
6.	Moderately stable (F)	$\sigma_\theta < 4$	i) Surface-based layer with flat top of depth within 100 m ii) Stratified layers of height less than 200 m	Clear night with strong radiative cooling and light/calm winds

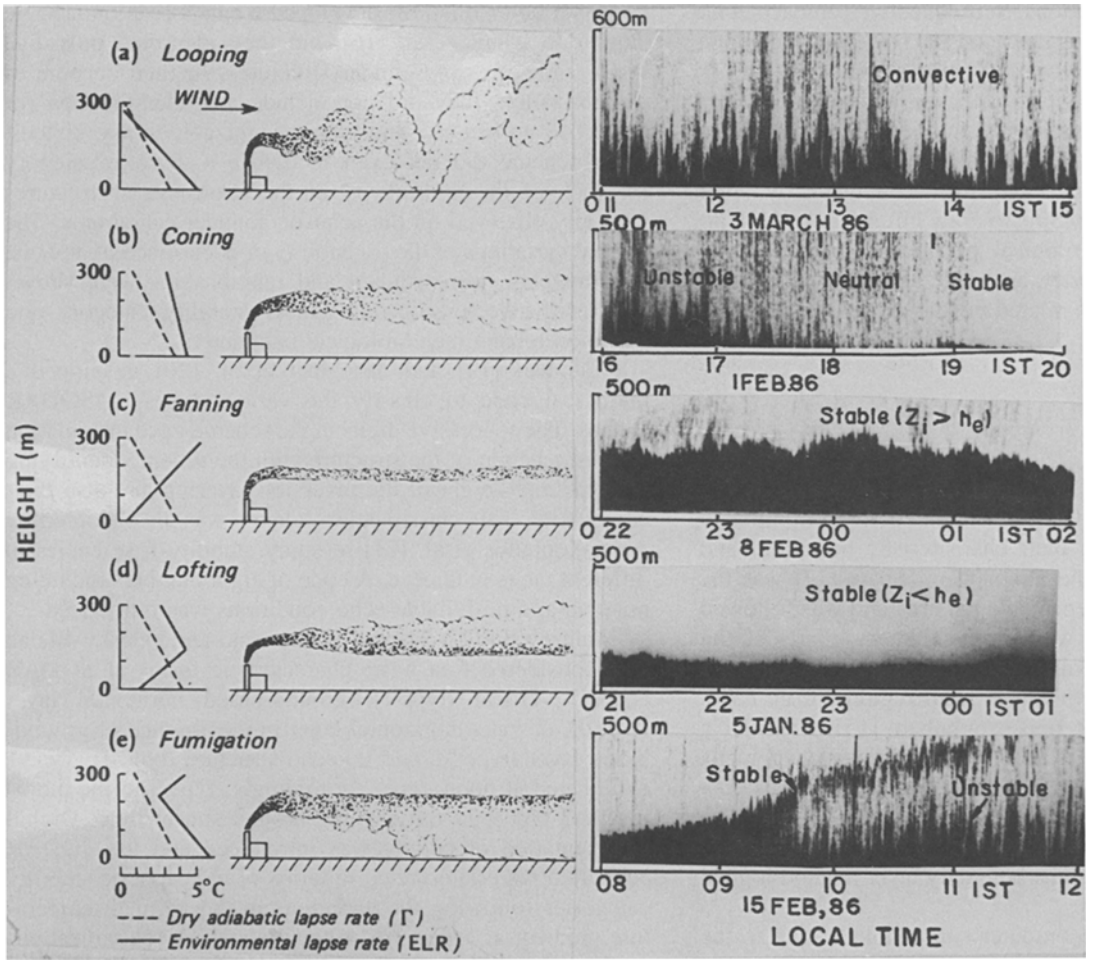

Fig. 4. Various lapse-rate conditions, behaviour of the stack plume and corresponding SODAR structures

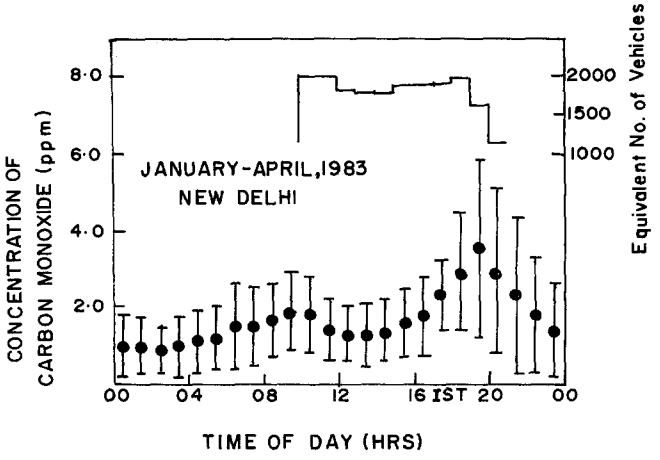

Fig. 5. Plot of the diurnal variations in the concentration of carbon monoxide and traffic density in New Dehli (India) as a function of the time of the day (hrs) marked in Indian standard time (IST)

stability classification. The characteristics of the SODAR echoes to classify Pasquill stability categories are given in Table 2. Singal and associates also correlated SODAR echo patterns obtained under various atmospheric conditions with lapse rate conditions and the associated stack plume behaviour. It was seen (Fig. 4) that looping under strong lapse-rate conditions (unstable weather) were linked with SODAR thermal plume structure, coning under sub-adiabatic conditions was associated with evening transition from unstable to stable weather conditions, fanning was a property of the stable weather when inversion depth was more than the height of the plume stack, lofting occurred under conditions of inversion depth less than the height of the plume stack and fumigation was the period of the morning eroding stable layer.

The above technique of determining Pasquill stability classification from the observed SODAR echogram characteristics was used by Singal et al. [30] to explain the distinct anomalous peaks (a weak one in the morning and a strong one in the evening) in the measured carbon monoxide concentration (Fig. 5) on the busy traffic roads of New Delhi due to vehicular traffic, although the same number of vehicles on average were passing the measurement place all through the day. It was found that the weaker morning peak lies during the fumigation period under unstable weather conditions while the stronger evening peak was due to the presence of stable weather conditions which did not help in the dispersion of carbon monoxide. Typical diurnal plots of the SODAR derived stability category and simultaneously measured concentration of carbon monoxide in the atmosphere near the ground surface for a set of days having different weather conditions (Fig. 6) further showed very clearly that the prevailing stability category determined the concentration of carbon monoxide present in the atmospheric air.

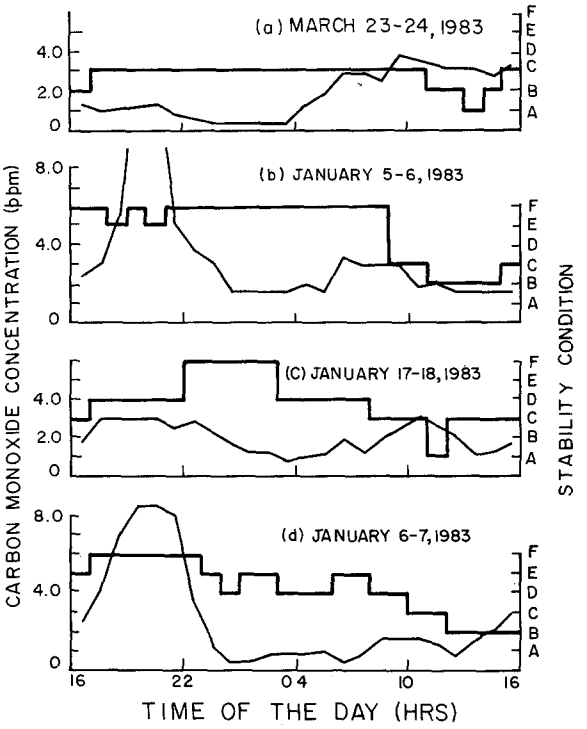

Fig. 6. Plot of simultaneously measured carbon monoxide (CO) concentration and SODAR observed atmospheric stability as a function of the time of the day. *Thick lines* represent stability conditions and *thin lines* represent CO concentration

This technique of stability classification was also used to determine the stability classes for any hour of the day for Ngawha Springs (New Zealand) [31] from the structural details of the monostatic acoustic sounder echograms obtained for the year 1983. However, exact height specification had to be worked out for this place since the terrain, latitudes and the system were different. The results were compared (Table 3) with the stability classes obtained for the respective hours using the technique developed by Wratt [32] based on calculating the bulk Richardson number using data from the 56 m instrumented tower operated simultaneously with the monostatic acoustic sounder at the same site. It was seen that tower and acoustic sounder stability schemes give a correlation for about 50% of the time. The correlation was found to become better in case limited classification of differentiating unstable, neutral and stable categories only was considered. This type of result is not surprising since the two methods for stability classification differ in the sensitivity range of the meteorological parameters. While the bulk Richardson number method is sensitive mainly to conditions within the surface layer (the lowest 50 m of the atmosphere), the acoustic sounder classification scheme uses information from well up in the mixed layer up to 700 m.

Foken et al. [33] considered ground-based structures, free structures (pattern not touching the ground), transition pattern, convective pattern, no echo, and disturbances of meteorological or technical origin as the basic SODAR structures and coded them by 2-digit code figures compatible with computer pattern recognition. The patterns were represented by the divided tens-figure with the first two basic patterns subclassified into internal (inhomogeneous) and multiple patterns for which unit figures were used to describe the necessary details. Height information of a pattern was further encoded by two digits for representing the lower and upper boundary of the phenomenon and two digits were used to describe the tendency of the development of the phenomenon with the intensity of a pattern encoded by a scale.

Evers et al. [34, 35] considering the two basic types of echo structures for the stable and unstable atmospheric conditions, defined the following distinct echo patterns:

L_G – Ground based compact structures,
L_E – Layer shaped elevated structures,
S – Spiky structure extending from the ground interspaced with blanks on the time axis,
X – Transition type between convection S and inversion L_G and L_E,
C – Echo structure with considerably varying local and temporal occurrence typical of frontal passages and precipitation,
NE – No echo due to missing turbulence in the $\lambda/2$ range.

It was noticed by them that convection in rural areas starts one hour later and ends one hour earlier than in the city. Further, the height of the structures L_G, L_E and X in rural locations is lower than in the urban areas. Based on the studies of diurnal variations in temperature gradients and radiation data, SODAR structures were used to identify three stability categories, stable, unstable and quasi-neutral, very clearly. The ground-based layer structures defined the stable category, the spiky structures defined the unstable category and the no echoes and transition echoes with small vertical extension defined the quasi-neutral category.

Based on the above echo patterns and their height and the measured radiation data, Neisser et al. [36] further defined all the seven stability classes. However, it was found that the error rate in the determination of stability

Table 3. Contingency table comparing sability classes from the tower and the acoustic sounder

		Stability class from tower data						Totals
		A	B	C	D	E	F	
Stability class from sounder data	A	5	19	61	7	0	0	92
	B	13	16	213	40	0	0	329
	C	32	89	446	325	3	9	904
	D	9	15	87	786	186	214	1297
	E	1	5	14	167	191	309	687
	F	2	2	20	145	338	808	1315
	Totals	62	193	841	1470	718	1340	4624

from SODAR data had a marked diurnal variation, with the discrepancy becoming largest at night with the stable stratification. These results suggested that the use of SODAR data for determining stability classes required more detailed investigations.

Neff and King [37] established stability regime classifications from the high resolution mini SODAR facsimile records while studying meteorology of high pollution episodes in the Denver, CO, metropolitan area. Structures pertaining to the surface mixing layer depth (the lowest uniform echo layer on the SODAR record), depth of the convective echoes, the height of a capping inversion, if any, and the maximum height of any continuously stratified echoes on the records were identified. A stability classification scheme was laid down which was based on the observation that conditions most conducive to limited vertical mixing were those in which there were the greatest number of fine stratified layers on the SODAR facsimile records. Three classes were marked, weak, moderate and strong, with finer gradations of +/− designation allowed for each class.

Neff [38] suggested a method, using the ratio of the acoustic backscatter and forward scatter intensities and a knowledge of the Richardson number, to estimate the temperature gradients and thus the stability. He expressed the temperature gradient $\delta\theta/\delta z$ as follows:

$$\delta\theta/\delta z = 0.0074\left[(1 - \mathrm{R_{if}})/\mathrm{R_{if}}\right]\left[\sigma_\mathrm{R}/(1.3 - \sigma_\mathrm{R})\right],$$

where σ_R represents the ratio of the backscatter to the forward scatter intensities from the same volume of the air and $\mathrm{R_{if}}$ represents the flux Richardson number. Since the scattering was maximum near the critical Richardson number, it was hypothesised that the temperature gradient can be estimated under conditions of the critical Richardson number. The method can be reliable since it eliminates calibration and attenuation errors, however, it has not been practically employed so far.

Doppler SODAR measured wind velocity can also be used to classify stability. In this respect Gland [39] and Jones et al. [40] proposed a simple model of determining stability, wherein the lowest layers of the atmosphere were classified either stable or unstable depending on the value of the standard deviation σ_W of the vertical wind speed. According to Gland if $\sigma_\mathrm{W} < 0.45\ \mathrm{m\ s^{-1}}$, the atmospheric conditions were classified as stable and if $\sigma_\mathrm{W} \geq 0.45\ \mathrm{m\ s^{-1}}$, unstable or neutral conditions were said to prevail. Jones et al. however, proposed the critical value of atmospheric stability switching at $0.3\ \mathrm{m\ s^{-1}}$. They also proposed a method of determining the top of the stable layer. According to them, the height of the successive horizontal velocity values where wind shear became maximum, was the top of the stable ground-based layer.

Thomas [41] presented two schemes of Pasquill stability classification based on Doppler SODAR data. According to one scheme, he used the standard deviation σ_W of vertical wind speed and the horizontal wind speed U at a height of 100 m to determine Pasquill stability classification and according to the other scheme, he used the standard deviation σ_ϕ of vertical wind direction and vertical profile of backscattered amplitude both measured at a height of 100 m. He found statistical equivalence of both these schemes with the classification scheme derived from the measurements of σ_ϕ by a vector vane at the 100 m level of the tower.

Best et al. [42] found that the use of σ_θ, the standard deviation of horizontal wind direction for stability determination, could be misleading in all but very flat and uniform terrain. For determining the stability at Stanwell (Australia), they preferred to use the turbulence parameter, σ_W/U. A comparative study of the stabilities determined by the two techniques is shown in Table 4. Gland [43] also considered, using the turbulence intensity parameter, σ_W/U for stability classification. On further studies, however, he found [39] that it was leading to unrealistic results in cases of weak wind associated with strong atmospheric stability.

4 Mixing Depth Studies

It has already been seen that a monostatic SODAR records thermal echoes during day time and shear echoes under stable weather conditions. We also know that SODAR echograms are a reflex image of turbulence in the lower atmosphere, i.e. echograms will not be traced unless inhomogeneities or turbulence in the thermal structure is present in the planetary boundary layer. Since turbulence in the lower atmosphere is responsible for dispersion of the effluents, therefore a measure of the height of the thermal plumes during day time and of the shear echoes during night time should give a measure of the mixing depth. Reliable measurements can, however, be made only for the period when ground-based shear echoes are present during night time or when an elevated capping layer is present above the thermal echoes during day time. The necessity of observing the elevated capping layer during daytime is due to the fact that the visible extent of the thermal plumes will mostly give an underestimate since it is a function of the SODAR sensitivity, a parameter dependent on the prevailing ambient noise.

Table 4. Estimated occurrence percentage of Pasquill stability classses for the Stanwell area using σ_θ and σ_w/U parameters. 10 m values of wind direction have been used for σ_θ while measured values from the Doppler acoustic sounder at 212 m have been used for determining vertical turbulence intensity parameter, σ_w/U. (Data from [42])

Stability class	From σ_θ		From σ_w/U	
	Criterion (degrees)	Estimated percentage	Criterion	Estimated percentage
A	>22.5	20.7	>0.15	29.4
B	17.5–22.5	8.0	0.1 –0.15	20.4
C	12.5–17.5	26.4		
D	7.5–12.5	27.5	0.05–0.1	41.0
E	3.5– 7.5	11.2	0.0 –0.05	9.4
F	0 – 3.5	6.2		

Since ambient noise is high during day time as compared to night time, SODAR sensitivity is low during day time.

Question also arises how far a measure of the height of the ground-based shear echoes compares with the height of the stable boundary layer (i.e. inversion height). At present there is no overall accepted definition for the stable boundary layer height. Different thermal, dynamical and turbulent depth scales have been proposed by various authors.

Extensive investigations have been made by many investigators to study and compare the SODAR determined height of the stable layer with that determined from a measure of the meteorological parameters. These studies, in brief, are as follows:

In a large number of preliminary investigations [34, 44–48], SODAR determined depth of the shear echoes was compared with the height of the ground based inversion layer reported by radiosonde. Considering the fast ascent rate of the radiosonde balloon near the ground level, the slow response of the sensors and the distance of the SODAR site from the radiosonde site, the small discrepancies in the two results were ignored and a good correspondence was generally reported.

Von Gogh and Zib [49] compared the simultaneous soundings of the lower atmosphere using monostatic acoustic sounder and tethered balloon borne sensors. Within the coincidence range (40–350 m) of the two systems, a good agreement between the soundings was reported in terms of the position of the statically stable zones in the atmosphere. The excellent agreement found between the simple dT/dz criterion and the position of acoustic scattering regions suggested that in the presence of inversion conditions, turbulent fluctuations sufficient to cause backscattering were invariably developed.

Russel and Uthe [50–52] made measurements of the mixing depth in the forenoon and during nocturnal inversion periods using SODAR and instrumented tower and aircraft and found that the two correlated well. The slightly increased scatter in the plots (Fig. 7) was attributed to frequent occurrence of several weak inversions or isothermal layers in the evening or night time temperature profiles.

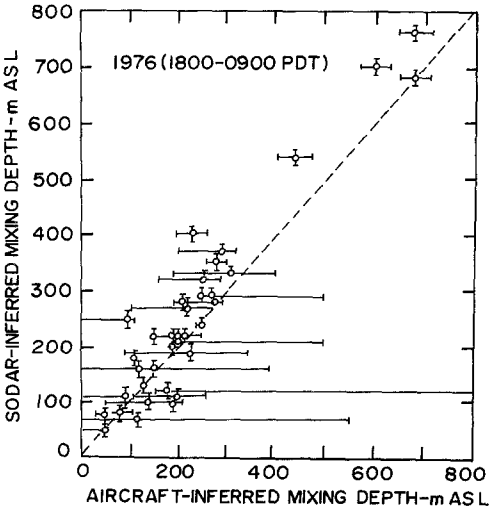

Fig. 7. Comparison of mixing depths inferred from SODAR and aircraft measurments. (Data from [51])

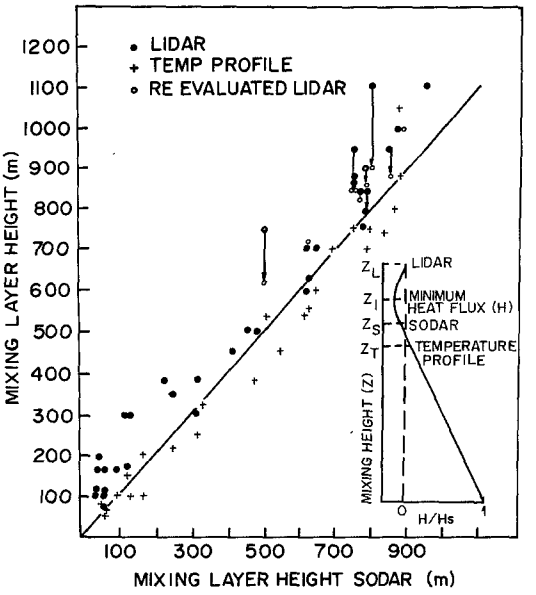

Fig. 8. Comparison of mixing layer heights determined by SODAR, LIDAR and temperature profiles. *Dots* represent LIDAR values, *plus signs* represents temperature profile values, *open circles* represent re-evaluated LIDAR values and arrows show their original point before re-evaluation. (Data from [53])

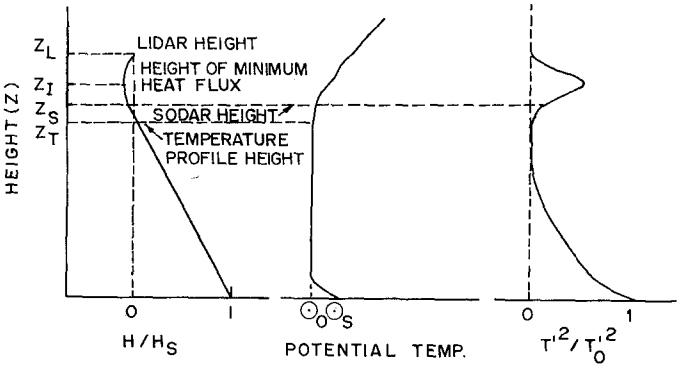

Fig. 9. Schematic showing difference in mixing layer heights determined using LIDAR (Z_L, temperature profile (Z_T and SODAR (Z_S. The height Z_I is the height of minimum heat flux. (Data from [53])

Coulter [53] compared mixing layer heights determined by temperature profile, LIDAR and SODAR observations in the forenoon under canopy conditions. He found that the overall values agreed fairly well but had systematic differences (Fig. 8). LIDAR derived values were consistently higher than SODAR derived values while temperature profile values were consistently lower than those estimated by the other two methods. These differences were attributed to the slightly different behaviour of the sensed variables near the capping inversion. Aerosols and particulate matter sensitive to LIDAR measurements mix to larger heights than the top of the adiabatic temperature profile, while temperature fluctuations sensitve to SODAR measurements exhibit an increase at a height above the top of the adiabatic temperature profile but below the maximum height of particulate mixing (Fig. 9)

Fitzharris et al. [54] described SODAR measurements of inversion frequencies near Cromwell (New Zealand) and

found that measured heights were comparable with those obtained from vertical temperature profiles from a kytoon capable of lifting temperature sensors up to 300 m above ground.

Walczewski [24] reported a correlation coefficient of 0.683 between the top of the ground-based SODAR echo layer and the top of the ground-based stable layer while making measurements in Cracow (Poland) in 1985 by monostatic SODAR and tethered balloon. On the basis of aircraft and acoustic sounder observations of O'Neil, Wangara, Mahrt et al. [55] found that, on the average, the top of the SODAR measured boundary layer occurred just below the low level wind maximum, which, in turn, approximately coincided with the height of the maximum in gradient Richardson number. Further, temperature inversion height was often around 25% higher than low level wind jet height.

Nieuwstadt and Driedonks [56] and Nieuwstadt [57, 58] reported that SODAR determined height of the turbulent layer under nocturnal stable conditions was usually smaller than that of the temperature inversion layer.

Arya [59] made detailed analysis of February 1975 Cabauw data for selected periods. A comparison of the SODAR measured height with other characteristic heights of the low level wind jet and of the potential temperature profile during nocturnal stable periods showed that the measured potential temperature profile had a poor correlation with SODAR determined height of the stable boundary layer and wind maximum height occurred at a lower height than the top of the SODAR measured height; on the whole for the very stable and extremely stable categories the height of the maximum in wind speed appeared to give a good agreement with the SODAR measured height. Considering all the data Arya also found that SODAR height was best correlated (coefficient of correlation 0.67) with the diagnostically determined heights obtained by using the relations given by Zilitinkevich [60] and Koracin and Berkowicz [61].

Beyrich [62] analyzed data of the HAPEX-MOBILHY experiment which was organized in the Landes forest region in the south-west of France in 1986. He found that the nocturnal surface inversion typically exhibited a layered structure on SODAR echograms of which the strongly stratified lower part was caused by cooling due to turbulent and radiational processes while the upper part with reduced temperature gradient was cooled by radiation only. Further, he found that SODAR observed height of the lower strongly stratified turbulent part of the surface inversion was equal to the stable boundary layer height of the surface inversion obtained in radio soundings. The coefficient of correlation was 0.90.

Koracin and Berkowicz [61], while examining SODAR measured height of the turbulent stable boundary layer, remarked that SODARS could yield mixing heights smaller than those relevant for air pollution modeling, since dispersion of pollutants was governed by velocity fluctuations in the nocturnal stable boundary layer while vertically operated SODAR was sensitive to temperature fluctuations whose magnitude decreased much faster with height than of velocity fluctuations. They further remarked that in the absence of any other more reliable measurements and considering the difficulties in the interpretation of SODAR measurements, SODAR measured height was the best measure of the turbulent stable boundary layer. In the same context, Caughey [63] had earlier remarked that it was very valuable to obtain a qualitative pictorial representation of the turbulent stable boundary layer from acoustic sounding in addition to the more usual highly detailed direct measurements of the flow.

The mixing height during daytime (unstable boundary layer) is the depth to the first elevated inversion layer from the ground level. It can be determined by locating the elevated inversion layer using the radiosonde data. Since radiosonde flights are routinely made only twice a day at location near the airports, for other times of the day and at inbetween stations, mixing height is estimated by applying the Holzworth model [64]. The mixing height during day time is generally up to 1–2 km.

Thermal echoes recorded on the SODAR facsimile records during day time cannot be directly used to determine mixing height since the height of the thermal echoes is dependent on SODAR sensitivity. Jones [65] suggested that capping layer if present above thermal plumes should invariably be used to estimate mixing height since the presence of a capping layer indicates the existence of a low level elevated inversion layer. This capping layer is generally present during morning hours and sometimes during day time also under certain conditions. In all other cases, the mixing depth would invariably lie beyond the range of the acoustic sounder. Jones arbitrarily suggested to use 1000 m as the mixing height in such cases.

Singal and associates [27, 66], using the Holzworth model, developed a technique to determine mixing height during day time when the plumes are not capped by a stable layer. Studies of the convective boundary layer on the basis of the Holzworth model using radiosonde data of New Delhi were made. This mixing height obtained from day-to-day was compared with the corresponding SODAR measured depth of the thermal plumes and an empirical relation as follows was laid down to determine the mixing height from the observed height of the thermal echoes:

$$h = 4.24 z_s + 95 ,$$

where h is the depth of the mixed boundary layer as per the Holzworth model and z_S is the depth of the sodar measured thermal plumes.

Weill et al. [67] found that the measurements of the Doppler velocities and their variance during the morning development of the convective boundary layer could be very useful for studying the convective structure and the mixing height under unstable conditions. Working at Chigne (France) they found that the profiles of the vertical velocity variance in free convection had a maximum at about half the height of the unstable boundary layer. This result was in agreement with the findings of Deardorff [68] and could thus help to define the altitude of the convective boundary layer at a place where heat flux vanished.

In a subsequent paper, Weill et al. [69] investigated the relationsheip between the height of the convective boundary layer and heat flux. They derived the following approximate equation under dry convective conditions during the morning development period:

$$\sigma_W^3 / Z \simeq (\alpha)^{3/2} (g/\odot) \overline{w' \odot'} ,$$

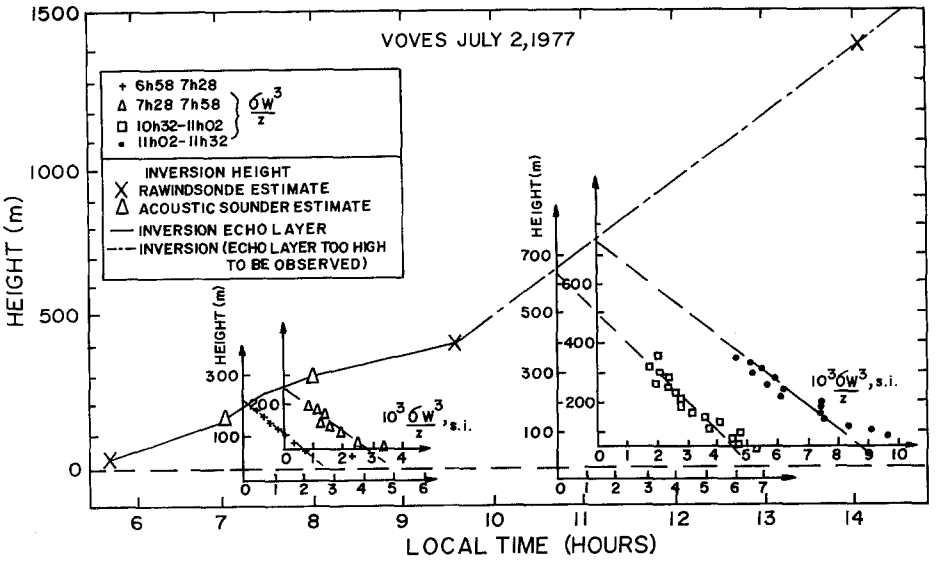

Fig. 10. Plots of the variation of the inversion height and σ_W^3/Z profiles. (Data from [67])

where Z is the height of the convective boundary layer, σ_W is the standard deviation of vertical velocity, w' is the vertical velocity perturbation, α is a constant approximately equal to 1.4, $\odot$ is the potential temperature, g is the acceleration due to gravity, and $\odot'$ is the fluctuation in potential temperature. Since this equation showed that sensible heat flux, $\overline{w'\odot'}$, was proportional to σ_W^3/Z, an attempt was, therefore, made to estimate the altitude of the convective boundary layer from the σ_W^3/Z profiles and the variation of the height of convective boundary layer in the morning development period. The plot (Fig. 10) showed that the estimated height of the convective boundary layer was close to the inversion height, Z_i, during the mornings and continued to remain measurable in the afternoon, offering thus an estimate of the mixing depth by the acoustic sounder in free convection. This result was, however, contradicted later on by Best et al. [70].

Melas [71] suggested similarity methods to measure surface heat flux and mixed layer depth in the CBL using capabilities of the acoustic sounder. An operational model based on Enger's work [72] was developed. It was shown that SODAR measurements of thermal structure parameter, C_T^2, and standard deviation of vertical wind σ_W, could be used to estimate the convective boundary-layer mixed-layer depth Z, and the surface heat flux Q_o, using the following relationships:

$$Z = (2.7/m)^{3/4}(g/T)^{-3/2}(C_T^2)^{-3/4}\sigma_W^3 z^{-1}\,,$$

$$Q_0 = 0.48\varphi C_p(g/\odot)^{1/2}(C_T^2)^{3/4}z\,,$$

where φ is the density of air, C_p is the specific heat at constant pressure, z is the height in the convective boundary layer where measurements are being made, m is a constant defined as $m = \sigma_W^2/W_*^2$ and is proposed to be equal to 0.45, and w_* is the mixed layer velocity scale.

The thermal structure parameter C_T^2 for the above computations will be determined from a knowledge of the relationship of C_T^2 with SODAR backscattering cross section $\sigma(\pi)$, which in turn will be computed from the received power for a backscattering acoustic sounding system defined by the SODAR equation as:

$$P_r = P_t\sigma(\pi)c\tau A_r(L_a/2R^2)\,,$$

where P_r and P_t are the received and transmitted acoustic power, respectively, τ is the transmitted pulse length, A_r is the area of the receiving antenna, R is the range to the scattering volume, and L_a is the atmospheric attenuation along the path taking into account the transducer efficiencies also.

In order to obtain absolute measurements of C_T^2, the SODAR has evidently to be calibrated acoustically and the excess acoustic attenuation has to be computed as a function of height. The excess attenuation is not well understood at the moment and can lead to large errors [73]. There have been a number of comparisons [4] of in situ measurements of C_T^2 with estimates of C_T^2 derived from SODAR measurements. Neff and Coulter [74] in their review paper have concluded that it is probably unrealistic to expect to obtain C_T^2 measurements better than within a factor of two, however, since vertical profiles of C_T^2 range over two orders of magnitude, they still can be useful.

The standard deviation of the vertical wind σ_W were computed from measurements of vertical wind using Doppler SODAR. There could be an uncertainty of about 30% in the measurements of σ_W but this uncertainty was very much reduced by averaging of the vertical variance in the mixed layer. A comparison between the direct measurements of mixed layer depth with SODAR estimates using the above approach showed a fair agreement with a correlation coefficient of 0.68. Uncertainty in SODAR estimates of C_T^2 was considered to be the major source of uncertainty in the mixed layer depth estimates.

5 Determination of Dispersion Coefficients

Gera and Singal [75] reported a technique to determine cross wind dispersion coefficient σ_y using SODAR data. Knowledge of bulk Richardson number deduced from a plot of the parameter for various heights of the boundary layer was used for this purpose.

The standard deviation of wind direction fluctuations σ_θ is related to the stability parameters Z/L through the relation [76]:

$$\sigma_\theta = aK(1 - bZ/L)/\left[\ln(Z/Z_0) + \beta(Z/L)\right],$$

where L defines the Monin-Obukhov length, a and b are the empirical constants and have the values $a = 1.5$ and $b = 1$ in stable conditions, and equal to 10 in unstable conditions, K is the von Karman's constant ($K = 0.4$), Z_0 is the length parameter of roughness and is approximately equal to 1.5 m for the centre of cities with tall buildings [77], and β is a constant and has a value equal to 6.

The stability parameter Z/L is related to the Richardson number R_i through the empirical results of Businger [78] and Pandolfo [79] as:

$R_i \approx Z/L$ (for unstable conditions)

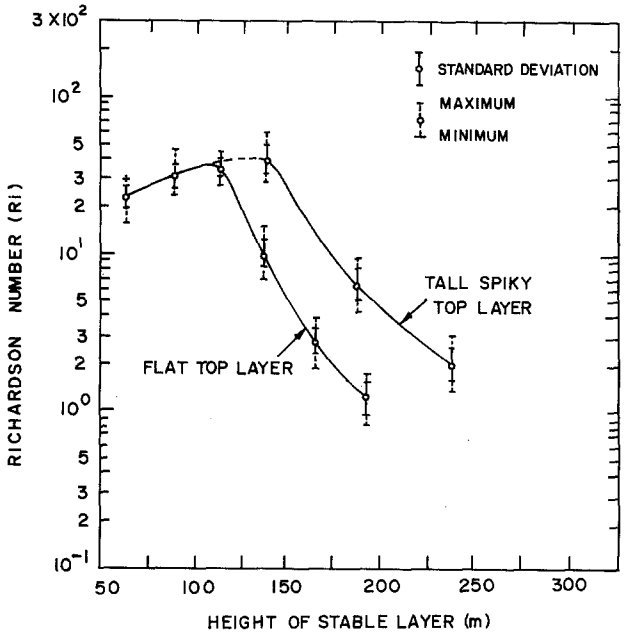

Fig. 11. A plot of the bulk Richardson number as a function of SODAR observed depth of the stable layer for flat top and tall spiky top structures

and

$R_i/(1 - 5R_i) = Z/L$ (for stable atmosphere).

The use of these relationships enabled the computation of σ_θ which in turn enabled to determine the horizontal dispersion coefficient σ_y through the use of the relation:

$$\sigma_\theta = \tan^{-1}(\sigma_y/x),$$

where x is the downwind distance in meters. Thus knowing R_i, one could estimate σ_y.

The scheme of working was first to plot the bulk Richardson number (from radiosonde data) at 00 GMT as a function of the corresponding depth of the stable boundary layer (from SODAR records) as shown in Fig. 11. This plot showed that the Richardson number first increased slightly with increasing depth of the stable boundary layer, arrived at a point of inflexion, beyond which it started decreasing steadily with increase in the depth of the stable boundary layer. The point of inflexion was more clear for the flat top stable structure. This plot was used to determine the prevailing value of the Richardson number for the given depth of the stable boundary layer and finally to compute σ_y.

A comparison of the computed values using the above scheme with those given by Pasquill-Gifford curves for stable conditions showed that the two agreed fairly well.

Vertical dispersion coefficient σ_z was computed from a knowledge of the cross wind horizontal dispersion coefficient σ_y using Martin's empirical relation [80]:

$$\sigma_y\sigma_z \cong 0.117(Q/U)\phi_{\max}.$$

Here Q is the quantity of emission measured in gs^{-1}, U is the wind speed (downwind) at the surface level measured in ms^{-1} and $\phi_{\max}$ is a function whose value is given in terms of downwind distance x as per Martin's nomograms (Fig. 12)

The vertical dispersion coefficient σ_z could also be computed as a function of downward distance x, in case the plume was actually passing over the sounder and could be visualized on the SODAR echograms. This has been practically done for the elevated dot echo structures observed

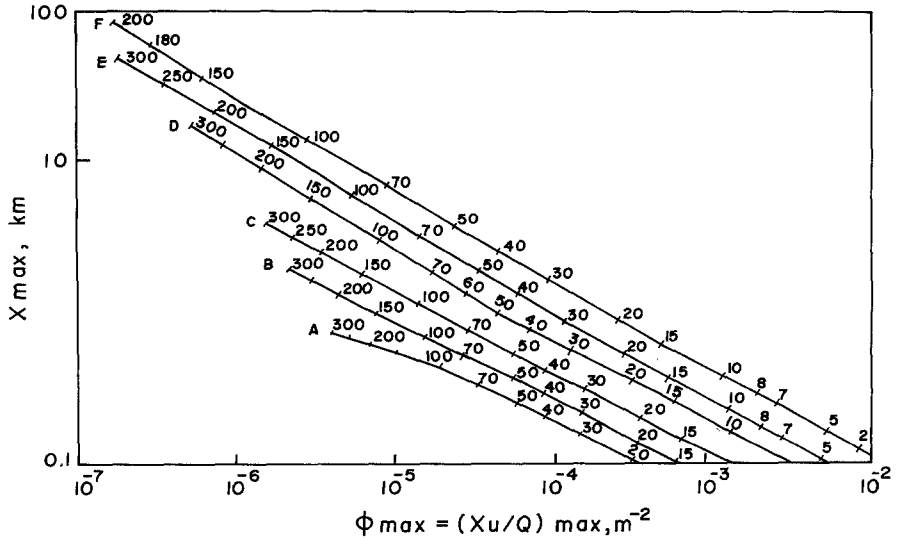

Fig. 12. Plot of the distance of maximum concentration and maximum xu/Q as a function of stability *(curves)* and effective height [m] of emssion *(numbers)*

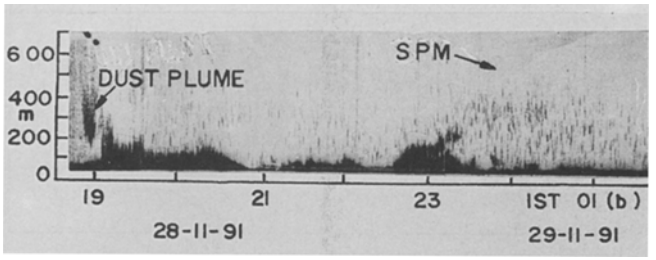

Fig. 13. A view of the SODAR echograms of elevated echo structures due to suspendend particulate matter (SPM) observed at Nimbahera, Chittorgarh (India)

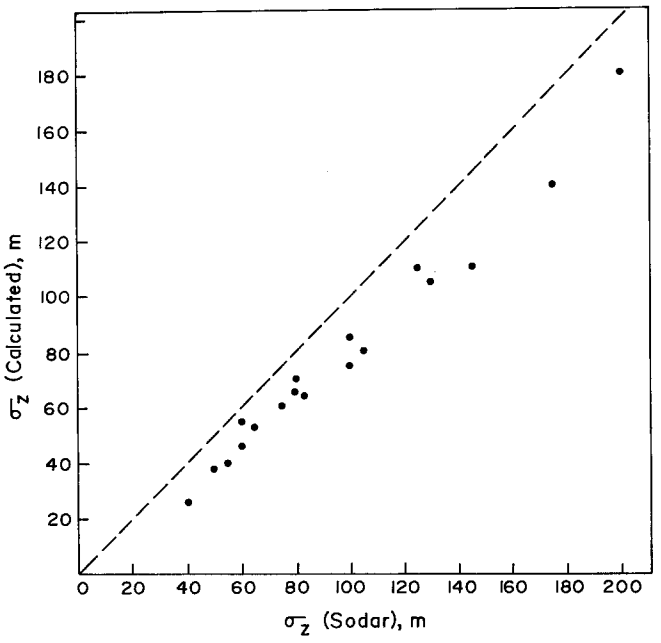

Fig. 14. A plot of the vertical dispersion coefficient, σ_z, obtained from SODAR echograms and Pasquill-Gifford curves

on the SODAR echograms (Fig. 13) on our sounder at Chittorgarh (India). These elevated structures were seen when the stack plume consisting of hot suspended particulate matter (SPM) from a nearby cement factory passed over the SODAR under favourable wind conditions. A comparison of these values of σ_z under C, D, and E stability categories with those obtained from Pasquill-Gifford curves showed (Fig. 14) that values obtained from SODAR echograms data were slightly higher (10–20%). This difference in the two values was possible since Pasquill-Gifford curves were valid for releases at 10 m level and for open terrain, while the release under consideration was at an elevated level in a complex semi-urban environment.

In the above context, it may be mentioned that Coulter and Underwood [81] had also shown, through measurements of the temperature structure parameter, the potential of the SODAR system to estimate relative dispersion coefficients of the cooling tower plume. They found that the width of the cooling tower plume increased linearly with distance from the tower and further it was broader (a factor of 2 to 5) on the acoustic sounder than observed visually.

6 Determination of Effective Stack Height

Effective stack height h_e (physical stack height plus plume rise height) for the emitted plume can be calculated using Holland's and Briggs' equations [80–82].

According to Holland's equation, the plume rise height Δh (m) is given as:

$$\Delta h = (U_z/U)D\left[1.5 + 2.68 \times 10^{-3} PD(T_s - T)/T_s\right],$$

where U_z is the wind speed at the stack height, T_s is the temperature of the effluent in the stack and D is the stack diameter. In this equation, the wind velocity U_z at the stack height can be estimated if needed in terms of the observed wind velocity at the surface level z_o by using the relation:

$$U_z = U(z/z_0)^p,$$

where p for the various stability conditions is given as:

	A	B	C	D	E	F
Urban	0.15	0.15	0.2	0.25	0.40	0.60
Rural	0.07	0.07	0.1	0.15	0.35	0.55

According to the Briggs equation the plume rise height Δh (m) is given as:

$$\Delta h = 1.6F^{1/3}U_z^{-1}d^{2/3} \quad \text{for } d \leq 3.5x^*$$

and $\Delta h = 1.6F^{1/3}U_z^{-1}(3.5x^*)^{2/3}$ for distances more than $3.5x^*$,

where $x^* = 14F^{5/8}$ if $F \leq 55$,

$x^* = 34F^{2/5}$ if $F > 55$,

$F = gV_sR_s^2[(T_s - T)/T_s]$ is the vertical flux of the bouyant plume,

V_s is the average exit velocity at the stack top in m s^{-1};

R_s is the inner stack radius at the top in m,

d is the distance from source to receptor in m, and

$3.5x^*$ is the distance to the point downwind of the stack where the plume is no longer rising.

The effective stack height can also be estimated from the SODAR observed elevated echoes on days of the stack plume passing over the sounder. In this case the central intense part of the elevated echo layer may be considered as the effective stack height.

The effective stack height calculated using the Briggs equation and estimated from SODAR records at Chittorgarh (India) have been compared. It may be seen (Fig. 15) that the effective stack height from the Briggs equations is lower by about 20% compared to that obtained from SODAR records. It is, however, well known that values obtained from the Briggs equation can have uncertainties up to 50%, therefore, the estimated values from SODAR records are in confirmity with those from the Briggs eqaution.

In the case of multiple stacks of nearly equal height located at different nearby places in a factory, the effective stack distance from the point of observation can also be estimated through geometrical configuration. Knowing the effective height of the various stacks, the various values of the dispersion coefficients σ_z for the actual distances

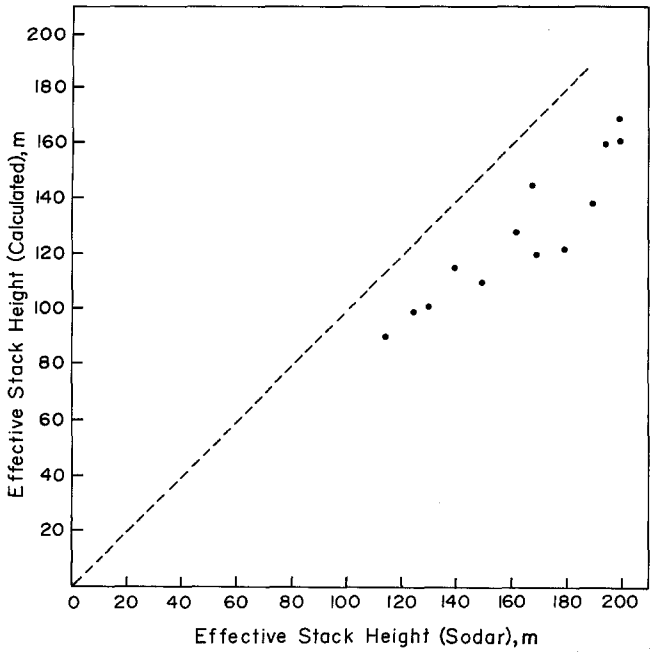

Fig. 15. A plot of the effective stack height estimated from SODAR elevated echo layer and calculated using the Briggs equation

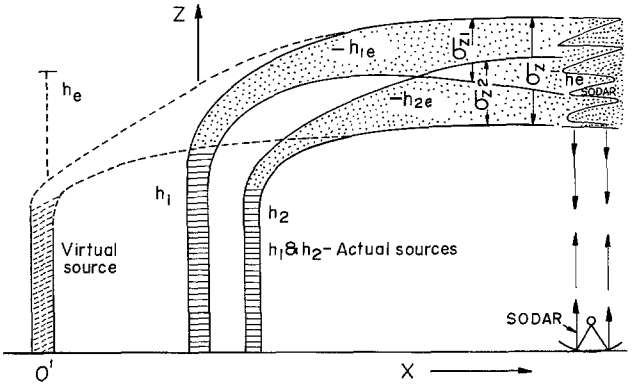

Fig. 16. Schematic for SODAR detection of effective stack height h_e, vertical dispersion coefficient σ_z and the location of the vertical source due to nearby multiple stacks

from the location of observation are plotted which merge into each other behaving effectively as if they are from a single virtual source (Fig. 16). The origin for the combined dispersion coefficient σ_z thus gives the effective distance of the multiple stacks from the point of observation.

7 Pollution Concentration Prediction

Very often it is desirable to estimate the pollution concentration at a place under different stability conditions for a given source or sources of emission. Efforts have also been made in this direction.

Jensen and Petersen [83] proposed a simple box model based on the height of the SODAR mixing layer to calculate air pollution concentrations and their variation in time. Concentrations of SO_2 in a large city (Gladsax, Denmark) during a subsidence situation were predicted and a good agreement (Fig. 17) between model results and measurements was found.

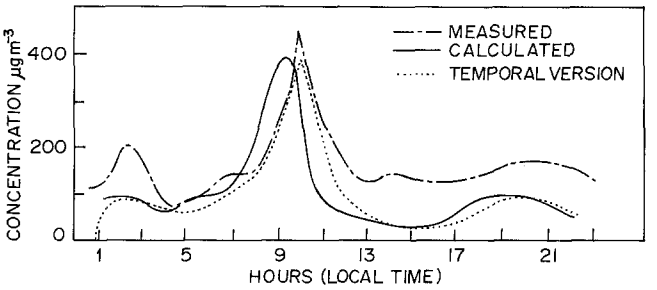

Fig. 17. Comparison of SO_2 concentrations measured on 20. Feb. 1975 at Gladsax TV tower (10 min average values) with those estimated using the simple quasi-stationary box model. (Data from [83])

Moulsley and Cole [84] showed that acoustic sounder measurements could be used to collect information about the size, behaviour and concentration of a methane plume released in the atmospheric air. For this purpose, concentration and wind velocity structure parameters of the methane plume were determined from acoustic scattering. Similar to the temperature structure parameter, the following equation for the back-scattering cross section $\sigma(\pi)$ in terms of the concentration structure parameter C_m^2 was derived:

$$\sigma(\pi) = 6 \times 10^{-4} k^{1/3} C_m^2 / P_0^2 .$$

Here P_0 is the total pressure. From the measurements, it was found that plume dimensions derived from sounder measurements agreed well with predictions of simple diffusion theory.

Brusasca et al. [85, 86] experimented feeding model input data from a Doppler acoustic sounder and radio acoustic sounding system installed near the power plant. They found that the performance of the simple Gaussian model improved through the use of data from the remote sensing systems and further that it paved the way to use more complex diffusion models.

Best et al. [42, 70, 87] reviewed air pollution dispersion models for convective conditions together with a discussion of the implications for power station siting, design and use of acoustic sounding data for a preferred dispersion model. It was found that for a given source location, acoustic sounder information was almost essential for the present level of understanding of convection at a complex non-ideal site.

Singal and associates [88] are also working at the National Physical Laboratory, New Delhi (India), to develop a SODAR based model to predict pollution concentration at a place due to a emission source, or sources. They propose to adopt the normal Gaussian dispersion model for estimating the downwind pollution concentration. The Gaussian dispersion model equations [80] under clear sky and canopy conditions are as follows:

For clear sky

$$\psi = (Q/2\pi\sigma_y\sigma_z U) \exp\left[-\frac{1}{2}(y/\sigma_y)^2\right] \times \exp\left[-\frac{1}{2}\left(\frac{z-h_e}{\sigma_z}\right)^2\right] \exp\left[-\frac{1}{2}\left(\frac{z+h_e}{\sigma_z}\right)^2\right].$$

Table 5. Stack data for the cement factory at Nimbahera

A. Kiln stacks	No.	1A	1B	2	3	4
All values at exit to atmosphere						
(i) Internal diameter [m]		1.6	1.2	2.2	2.2	3.0
(ii) Height above G.L. [m]		49.4	52.8	60.0	65.0	87.9
(iii) Stack gas temp. [° C]		140.0	140.0	150.0	150.0	300.0
(iv) Stack gas velocity [m/s]		15.0	26.0	20.0	20.0	27.0
(v) S.P.M.[a] concentration [mg/nm^3]		200.0	200.0	200.0	200.0	300.0
B. Cement mill stacks	No.		1	2	3	4
(i) Internal diameter [m]			0.6	0.6	0.6	0.9
(ii) Height above G.L. [m]			30.0	30.0	30.0	30.0
(iii) Stack gas temp. [° C]			90.0	90.0	100.0	100.0
(iv) Stack gas velocity [m/s]			12.0	12.0	14.0	12.0
(v) S.P.M.[a] concentration [mg/nm^3]			150.0	150.0	250.0	250.0
C. Other stacks			(a)		(b)	
(i) Height above G.L. [m]			60.0		40.0	
(ii) No. of stacks			6		8	
(iii) Internal diameter [m]			0.3		0.4	
(iv) Stack gas temp. [° C]			40.0		40.0	
(v) Stack gas velocity [m/s]			8.0		8.0	
(vi) S.P.M.[a] concentration [mg/nm^3]			150.0		150.0	

[a] S.P.M. – Suspended Particulate Matter

For canopy conditions, assuming that the downwind distance is more than the height of the elevated inversion base

$$\psi(x, y, z, h_e) = (Q/(2\pi)^{1/2}\sigma_y Z_i U) \exp\left[-\frac{1}{2}(y/\sigma_y)^2\right].$$

In these equations ψ is the pollution concentration at a place [g m^{-3}], x, y, z are the coordinates [m] and h_e is the effective stack height [m].

As a case study, the above approach has been applied to compute particulate matter concentration with respect to distance for a cement factory located at Nimbahera (Chittorgarh) in Rajasthan, India. The terrain is a vast valley sourrounded by medium range hills, a part of the Aravali mountains. The nearest hills are at a distance of around 10 km from the site. SODAR was placed at a distance of 500 m from the stacks. It has a range of 700 m and was operated for the period May 1991 to April 1992 taking sample data for about 10 days every month. The stack parameters are given in Table 5.

The Gaussian dispersion model equation used to determine the downwind concentration (surface level) of the particulate matter due to emission from a source gets slightly modified in this case and becomes:

$$\psi = (Q/\pi\sigma_y\sigma_z U) \exp\left[-\frac{1}{2}(y^2/\sigma_y^2 + h_e^2/\sigma_z^2)\right].$$

For carrying out the concentration calculations, the dispersion coefficients have been taken from the Pasquill-Gifford curves for the respective stability category determined from SODAR echograms and then suitably modified as per findings discussed in the previous sections. Calculations have been made for two locations, Gambhiri and Nimbahera, as shown in the layout map in Fig. 18. Results of the observed and calculated values for these two sites for each sampling period are given in Table 6 which also gives the sampling time of the observed particulate matter. (It may be pointed out that high volume sampler were used to measure particulate matter concentrations at a few selected places and further that sampling for the time period 17:00 h on one day to 9:00 hrs on the other day for the reported values at Gambhiri was continuous.) It may be seen that the model calculated values are more or less comparable with the observed values. The slight mismatch is considered to be due

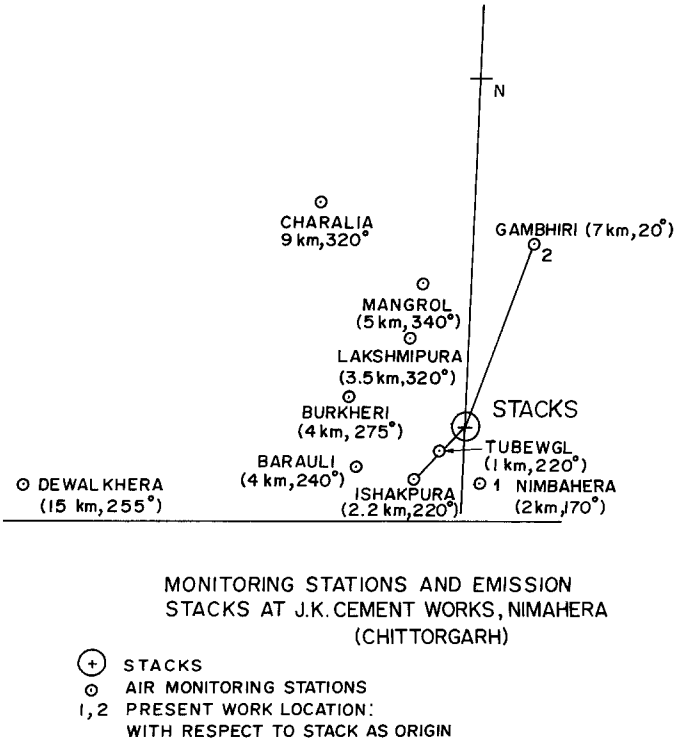

Fig. 18. Layout map of the sorroundings of J.K. Cement Works at Nimbahera (Chittorgarh) marking the site of SODAR location and the two other sites where particulate matter concentrations were measured. In the *brackets* at each site are given the respective distance and angle held with the source at the facxtory site

Table 6. Comparison of observed and calculated values of the particulate matter for the two locations

Location	Date	Sampling period (hrs)	Particulate concentration ($\mu g/m^3$)		Remarks
			Observed	Calculated (NPL model)	
Nimbahera	2-12-91	09h17	610	462	Possibility of local dust contribution
Gambhiri	30-11-91	17h00	94[a]	79	–do–
	1-12-91	00h09	94[a]	67	
	1-12-91	17h00	111[a]	121	Sampler not operative for part of the time
	2-12-91	00h09	111[a]	183	

[a] Continuous sampling from 17:00 hrs on one day to 09:00 hrs on the next day

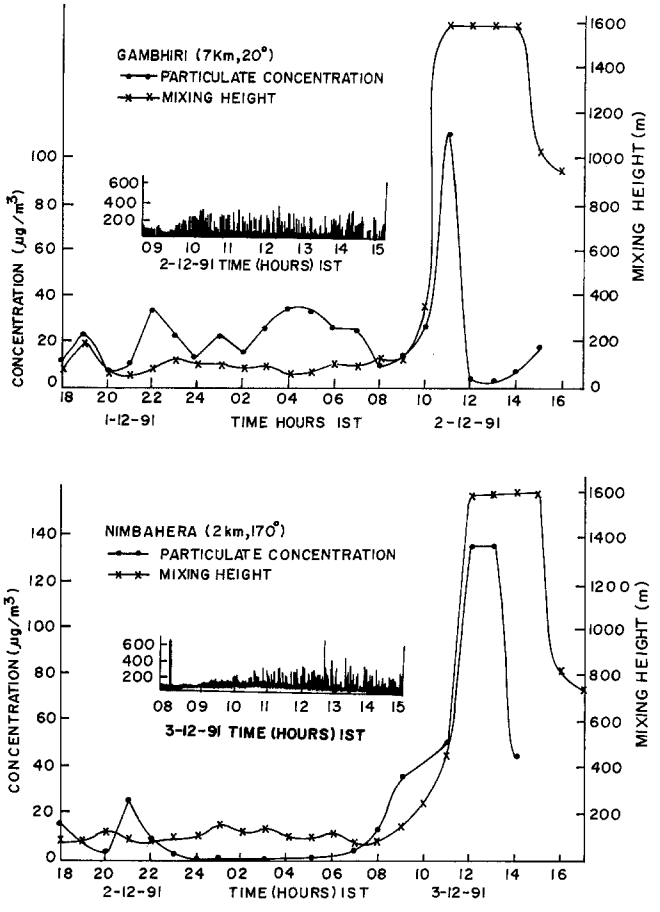

Fig. 19a, b. Studies of diurnal variations of computed concentrations of particulate matter in relation to SODAR derived mixing height at (**a**) Gambhiri (Chittorgarh) and (**b**) Nimbahera (Chittorgarh). The overlaid small diagrams are the diurnal variations in the SODAR echograms at the SODAR site near the cement factory showing the fumigation period followed by clear thermal plumes

to the possibility of local dust contribution and power failure during the sampling period.

Diurnal variations in the computed concentration of the particulate matter have also been studied in correlation with the SODAR determined mixing height for the above discussed two locations (Fig. 19). It may be seen that during the fumigation period (depicted by SODAR echograms as the morning rising layer from the surface level), the model computed concentration of the particulate matter increases enormously as expected.

8 Concluding Remarks

Low level radiosonde, tower, instrumented aircrafts, SODAR, LIDAR, and radio acoustic sounding system (RASS) are some of the most suitable instruments for measurements in the atmospheric boundary layer. The classical direct methods using radiosondes, highmasts, aircrafts etc. though, are very precise and reliable but are not adequate for obtaining full information and at the same time are very expensive to operate. Amongst the indirect remote instruments, SODARs probably are the most suitable, reliable and inexpensive instruments available for monitoring air pollution transport, atmospheric stability and height of the turbulent atmospheric boundary layer on a continuous basis. They deliver variances of vertical velocity and horizontal wind direction, data which are very useful for air pollution dipersion problems particularly for short range diffusion. It is now believed that SODARs are particularly well-suited for problems relating to high stack performance in power plants, mine siting, flow in complex terrain environments, and pollution episode monitoring and prediction. Further, SODAR measurements can be particularly effective in complex terrain since SODAR estimates of boundary layer parameters are better representative than direct measurements due to their being volume average and therefore less sensitive to local conditions.

A major shortcoming of SODARs is their limited vertical range which is well below the typical midday mixing heights and the poor quality in the measured wind variance σ_v, the standard deviation of the crosswind component [89]. It is still a challenge to determine dependable values of surface fluxes of momentum and heat using SODAR data. SODAR measurements of the temperature structure parameter C_T^2 are also contaminated with some inherent errors since reflectivity calibration for received power information requires measurements of humidity and temperature profiles, acoustic calibration of the transducer efficiency and a precise knowledge of acoustic attenuation, data which are not readily available.

Moulsly et al. [90] have shown that humidity present in the lower atmosphere can be measured using multi-frequency soundings, of course, the magnitude of the excess attenuation for this purpose should be known correctly. The errors can be reduced in case wide frequency spacings are used to obtain large attenuation differences. Operating with the mini SODAR at frequencies of 2048, 4681 and 6554 Hz, they reported that humidity measurements should be possible over a height range of 50–150 m with an error of 1–2 hPa.

Temperature measurements using acoustic sounding have also been reported. Fiocco et al. [91] have demonstrated the possibility of extracting temperature information from a measure of vertical acceleration using a vertically pointing tripple Doppler SODAR. Besides, RASS has now become available to extract atmospheric temperature information. Sound waves of frequencies 85 Hz to 1 kHz have been used for measuring temperature profiles with fairly good accuracy to heights generally up to 1 km with an upper limit of 30 km [92–96].

In short, it can be stated that, inspite of certain shortcomings, acoustic sounding through the years has gained recognition as an effective tool for remote measurement of meteorological parameters in the atmospheric boundary layer. The system is being used as a research tool as also is finding extensive use in air quality work. Indeed, SODAR today is one of the instruments available for monitoring air pollution related meteorology on a continuous basis.

Acknowledgements. The author thanks his colleagues Dr. B.S. Gera and Mr. D.R. Pahwa for helping him in the preparation of this paper. Thanks are also due to Director, National Physical Laboratory, New Delhi for permitting to publish this paper.

References

1. C.G. Little: Proc. IEEE **57**, 571 (1969)
2. E.H. Brown, F.F. Hall, Jr.: Rev. Geophys. Space Phys. **16**, 47 (1978)
3. W.D. Neff, R.L. Coulter: Acoustic remote sensing. In *Probing the Atmospheric Boundary Layer*, ed. by D.H. Lenschow (Amer. Meteorol. Soc., Boston, MA 1986) pp. 201–236
4. S.P. Singal: Acoustic sounding stability studies. In *Encyclopedia of Environmental Control Technology, Air Pollution Control*, ed. by P.N. Cheremissinoff (Gulf Publishing, USA 1989) pp. 1003–1061
5. W.D. Neff: Remote sensing of atmospheric processes over complex terrain. In *Meteorological Monographs - Atmospheric Processes over Complex Terrain*, ed. by W. Blumen (Amer. Meteorol. Soc., Boston, MA 1990) pp. 173–228
6. G.W. Gilman, H.B. Coxhead, F.H. Willis: J. Acoust. Soc. Am. **18**, 274 (1946)
7. L.G. McAllister: J. Atmos. Terr. Phys. **30**, 1439 (1968)
8. M.L. Wesely: J. Appl. Meteorol. **15**, 43 (1976)
9. S.K. Aggarwal, S.P. Singal, R.K. Kapoor, B.B. Adiga: Boundary-Layer Meteorol. **18**, 361 (1980)
10. D.W. Beran, F.F. Hall, Jr. J.W. Wescott, W.D. Neff: Application of an acoustic sounder to air pollution monitoring. In *Proceedings Symposium on Air Pollution Turbulence and Diffusion*, ed. by H.W. Church, R.E. Luna (Sandia Laboratories, Alburquerque, NM 1972) pp. 66–72
11. I. Tombach, P.B. Mac Cready, L. Baboolal: Use of a monostatic acoustic sounder in air pollution diffusion estimates. J. Instrum. Soc. Am., 139–149 (1973)
12. N.A. Shaw: *Acoustic sounding of the atmosphere*. Dissertation, University of Melbourne (1971)
13. M. Fukushima: J. Radiat. Res. Labs. J. **22**, 23 (1975)
14. M. Fukushima: J. Radiat. Res. Labs. J. **22**, 151 (1975)
15. J.F. Schubert: A climatology of the mixed layer using acoustic methods. In *Proceedings of the 3rd Symp. on Meteorological Observations and Instrumentation* (American Meteorological Society, Washington, DC (1975) pp. 151–156
16. G.H. Clark, E. Chanash, E.O.K. Bendun: J. Appl. Meteorol. **16**, 1365 (1977)
17. F.C. Hall, Jr.: Boundary layer climatologies from acoustic sounder investigations. In *Proc. 4th Symposium on Meteorological Observation and Instrumentation* (American Meteorological Society, Denver, CO. 1978) pp. 330–332
18. B.E. Prater, J.J. Colls: Atmos. Environ. **15**, 793 (1981)
19. R.A. Maughan: Atmos. Environ. **13**, 1697 (1979)
20. R.A. Mauaghan, A.M. Spanton, M.L. Williams: Atmos. Environ. **16**, 1209 (1982)
21. D.N. Asimakopoulos, G.G. Helmis, D.G. Deligiorgi: Classification of acoustic sounder facsimile records for use in air pollution experiments. In *Proc. Int'l Meeting on Application of SODAR and LIDAR Techniques in Air Pollution Monitoring* (EURASAP) (Krakow, Poland 1990) pp. 1–7
22. J. Walczewski: Acoustic sounding of the atmosphere for inversion layer climatology over an urban area. In *Proc. 2nd Int'l Symp. on Acoustic Remote Sensing of the Atmosphere and Oceans* (Rome, Italy 1983) pp. XXII 1–16
23. J. Walczewski: Characteristics of the boundary layer of the atmospher over Cracow on the basis of the results of acoustic sounding. In *Research Papers of the Institute of Meteorology and Water Management*. Warsaw, Poland, Ser. Meteorology, Vol. 10 (1984)
24. J. Walczewski: Z. Meteorol. **39**, 129 (1989)
25. J. Walczewski, M. Felesky-Bielak: Atmos. Environ. **22**, 1793 (1988)
26. S.P. Singal, B.S. Gera, S.K. Aggarwal: Studies of the boundary layer at Delhi using Sodar. In *Proc. Second Int'l Symp. on Acoustic Remote Sensing of the Atmosphere and Oceans* (Rome, Italy 1983) pp. XXIII 1–8
27. S.P. Singal, B.S. Gera, S.K. Aggarwal: J. Sci. Ind. Res. **43**, 469 (1984)
28. S.P. Singal, S.K. Aggarwal, D.R. Pahwa, B.S. Gera: Atmos. Environ. **19**, 221 (1985)
29. S.P. Singal: Need for acoustic sounding (SODAR) monitoring of the atmospheric boundary layer for environmental pollution management. In *Environmental Planning and Management in India*, ed. by R.K. Sapru, Vol. 1 (Ashish, New Delhi 1990) Chap. 10, pp. 79–105
30. S.P. Singal, S.K. Aggarwal, B.S. Gera, D.R. Pahwa, Mukesh Sharma: Atmos. Res. **20**, 133 (1986)
31. S.P. Singal, E.W.D. Lewthwaite, D.S. Wratt: Atmos. Environ. **23**, 2079 (1986)
32. D.S. Wratt: Atmos. Environ. **21**, 2599 (1987)
33. T. Foken, K.H. Hartmann, J. Keder, W. Kuchler, J. Neisser, F. Vogt: Z. Meteorol. **35**, 348 (1987)
34. K. Evers, J. Neisser, E. Weiss: Z. Meteorol. **37**, 241 (1987)
35. K. Evers, J. Neisser: Atmos. Environ. **24** A, 2541 (1990)
36. J. Neisser, G. Bull, K. Evers, M. Weimann, E. Weiss, J. Keder, I.V. Petenko: Results of sodar investigations of the structure of the planetary boundary layer. In *Proc. of the Field Experiment Kopex-86* (Czechosl. Acad. Sci. Prague 1988) pp. 109–141
37. W.D. Neff, C.W. King: The use of sodars in an urban air quality study. In *Acoustic Remote Sensing*, ed. by S.P. Singal (Tata McGraw-Hill, New Delhi 1990) pp. 506–512
38. W.D. Neff: An Observation and numerical study of the atmospheric boundary layer overlying the east antartic ice sheet: NOAA Tech. memo. ERL WPL-67 (NTIS PB81-21196) Wave Propagation Laboratory, Boulder, CO. 1981) pp. 272
39. H. Gland: Qualifying test on a three dimensional Doppler SODAR: Report HE/32-81.9, (French Electricity Board, Department of Aquatic and Atmospheric Environment, Division of Applied Meteorology and Atmospheric Pollution Paris, France 1981) pp. 35
40. D.E. Jones, P.J. Smith, N.A. Shaw, I.A. Bourne: Analysis of acoustic radar wind data. In *Proc. Eighth Int'l Clean Air Conference*, Melbourne, (1984) pp. 337–349
41. P. Thomas: Atmos. Res. **20**, 165 (1986)
42. P.R. Best, M. Kanowski, L. Stumer, D. Green: Atmos. Res. **20**, 173 (1986)
43. H. Gland: Experiments with a Doppler acoustic sounder. Report HE/32-80.24 (French Electricity Board, Department of Aquatic and Atmospheric Environment, Division of Applied Meteorology and Atmospheric Pollution, Paris, France 1980) pp. 33
44. R.J. Wyckoff, D.W. Beran, F.F. Hall: J. Appl. Meteorol. **12**, 1196 (1973)
45. H. Parry, C.M. Sanders, H. Jensen: J. Appl. Meteorol. **14**, 67 (1975)
46. A.K. Goroch: J. Appl. Meteorol. **15**, 520 (1976)

47. R.B. Hicks, D. Smith, P.J. Irwin, T. Mathews: Boundary-Layer Meteorol. **12**, 201 (1977)
48. S.P. Singal, S.K. Aggarwal: Indian J. Radio Space Phys. **8**, 76 (1979)
49. R.G. von Gogh, P. Zib: J. Appl. Meteorol. **17**, 34 (1978)
50. P.B. Russel, E.E. Uthe: Sodar network measurements of regional mixing depth and stability patterns for an air quality model. In Preprints of the *Fourth Symp. on Meteorological Observations and Instrumentation* (Amercian Metorological Society, Denver, CO 1978) pp. 490–497
51. P.B. Russell, E.E. Uthe: Bull. Am. Meteorol. Soc. **59**, 1275 (1978)
52. P.B. Russell, E.E. Uthe: Atmos. Environ. **12**, 1061 (1978)
53. R.L. Coulter: J. Appl. Meteorol. **18**, 1495 (1979)
54. B.B. Fitzharris, A. Turner, W. McKinley: N. Z. J. Sci. **26**, 307 (1983)
55. L.J. Mahrt, R.C. Heald, D.H. Lenschow, B.B. Standlov, I. Troen: Boundary-Layer Meteorol. **17**, 247 (1979)
56. F.T.M. Nieuwstadt, A.G.M. Driedonks: J. Appl. Meteorol. **16**, 115 (1979)
57. F.T.M. Nieuwstadt: Boundary-Layer Meteorol. **20**, 3 (1981)
58. F.T.M. Nieuwstadt: Boundary-Layer Meteorol. **30**, 31 (1984)
59. S.P.S. Arya: J. Appl. Meteorol. **20**, 1192 (1981)
60. S.S. Zilitinkevich: Boundary-Layer Meteorol. **3**, 141 (1972)
61. D. Koracin, R. Berkowicz: Boundary-Layer Meteorol. **43**, 65 (1988)
62. F. Beyrich: Some questions of mixing height determination from sodar observations. In *Proc. 6th Int'l Symp. on Acoustic Remote Sensing and Associated Techniques of the Atmosphere and Oceans* (Athens, Greece 1992) pp. 205–211
63. S.J. Caughey: Observed characteristics of the atmospheric boundary layer. In *Atmospheric Turbulence and Air Pollution Modelling*, ed. by F.T.M. Nieuwsatdt, H. Van Dop (Reidel, Dordrecht 1982) pp. 107–158
64. G.C. Holzworth: J. Appl. Meteorol. **6**, 1039 (1967)
65. D.E. Jones: Clean Air **19**, 49 (1985)
66. S.P. Singal, S.K. Aggarwal, B.S. Gera: J. Sci. Ind. Res. **39**, 73 (1980)
67. A. Weill, L. Eymard, M.E. Lequere, C. Klapisz, F. Baudin, P. Van Grunderbeeck: Investigations of the planetary boundary layer with an acoustic Doppler sounder. In *Proc. 4th Symp. on Meteorological Observations and Instrumentation* (American Meteorological Society, Denver, CO 1978) pp. 415–421
68. J.W. Deardorff: Three dimensional and numerical modelling of the planetary boundary layer. In *Workshop on Micro-Meteorology*, ed. by D.A. Haugen (American Meteorological Society, Boston, MA 1972) pp. 271–309
69. A. Weill, C. Klapisz, B. Strauss, F. Baudin, C. Jaupart, P. Van Grunderbeeck, J.P. Goutorbe: J. Appl. Meteorol. **19**, 199 (1980)
70. P.R. Best, J. Ewald, M. Kanowski: The estimation of pollutant dispersal from Queensland Power Station. In *Proc. 7th Int'l Clean Air Conference*, ed. by K.A. Webb and A.I. Smith (Clean Air Society of Australia and New Zealand, Adelaide, Australia 1981) pp. 429–448
71. D. Melas: Atmos. Environ. **24** A, 2847 (1990)
72. L. Engler: Atmos. Environ. **24** A, 2457 (1990)
73. D.A. Haugen, J.C. Kaimal: J. Meteorol. **17**, 895 (1978)
74. W.D. Neff, R.L. Coulter: Acoustic remote sensing. In *Probing the Atmospheric Boundary Layer*, ed. by D.H. Lenschow (AMS Boston, MA 1986) pp. 201–239
75. B.S. Gera, S.P. Singal: Atmos. Environ. **24** A, 2003 (1990)
76. K. Takeuchi: J. Meteorol. Soc. Jpn. **1**, 40 (1962)
77. ESDU: *Characteristics of atmospheric turbulence near the ground*, Part 3: Variations in space and time for strong winds (neutral atmosphere), Item 75001, 1–27 (1976)
78. J.A. Businger: Transfer of heat and momentum in the atmospheric layer. In Prog. Arct. *Heat Budget and Atmospheric Circulations*, Santa Monica, CA, Rand Corp. 305–332 (1968)
79. J.P. Pandolfo: J. Atmos. Sci. **23**, 495 (1966)
80. D,B, Turner: *Workbook of Atmospheric Dispersion Estimates*: Pub. No. AP-26 (Office of Air Programs, Environmental Protection Agency, USA 1970)
81. R.L. Coulter, K.H. Underwood: J. Appl. Meteorol. **19**, 1395 (1980)
82. G.A. Briggs: Plume rise predictions. In *Lectures on Air Pollution and Environmental Impact Analysis*, ed. by D.A. Haugen (A.M.S. Boston 1975) pp. 59–111
83. N.O. Jensen, E.L. Petersen: Atmos. Environ. **13**, 717 (1979)
84. T.J. Moulsley, R.S. Cole: Atmos. Environ. **14**, 1063 (1980)
85. G. Brusasca, G. Elisey, M. Maini, A. Marzorati: Acoustic remote sensing for environment control in thermal power plants. In *Proc. 2nd Int'l Symp. on Acoustic Remote Sensing of the Atmosphere and Oceans* (Rome, Italy 1983) pp. XXI, 1–12
86. G. Brusasca, P. Groppelli, G. Tinarelli: Central intelligent unit for atmospheric pollution control using remote sensing measurements. In *Proc. 3rd. Int'l Symp. on Acoustic Remote Sensing of the Atmosphere and Oceans* (Issy-les-Moulineaux, France 1985) pp. 527–550
87. P.R. Best, M. Kanowski, P. Morland, L. Stumer: A comparison of acoustic sounder statistics at various sites on the Australian Continent. In *Proc. 2nd. Int'l Symp. on Acoustic Remote Sensing of the Atmosphere and Oceans* (Rome, Italy 1983) pp. XXXIV, 1–24
88. S.P. Singal, B.S. Gera, D.R. Pahwa: Application of sodar to air pollution meteorology. Int. J. Remote. Sensing (1993), in press
89. J.E. Gaynor, C.B. Baker: Quantifying errors in sodar wind variance measurements. In *Proc. 6th. Int'l Symp. on Acoustic Remote Sensing and Associated Techniques of the Atmosphere and Oceans* (Athens, Greece 1992) pp. 47–52
90. T.J. Moulsley, D.N. Asimakopoulos, R.S. Cole, S.J. Caughey: Atmos. Environ. **16**, 1501 (1982)
91. G. Fiocco, M.G. Ciminelli, G. Mastrantonio: Atmos. Res. **20**, 199 (1986)
92. V.D. Belyavskaya, M.A. Kallistratova, G.A. Karyukin, I.V. Petenko: Izv. Atmos. Ocean Phys. **20**, 277 (1984)
93. G. Bonio, P.P. Lambardini, A. Longhetto, P. Trivero: Nature **290**, 121 (1981)
94. G. Peters, H. Timmerman, H. Hinzpeter: Int. J. Remote Sensing **4**, 49 (1983)
95. M. Matuura, Y. Masuda, H. Inuki, S. Kato, S. Fukao, T. Sato, T. Tsuda: Nature **323**, 426 (1986)
96. P.T. May, K.P. Moran, R.G. Strauch: J. Appl. Meteorol. **28**, 1329 (1989)